The Mexican hat wavelet family: application to point-source detection in cosmic microwave background maps

J. González-Nuevo,[1]⋆ F. Argüeso,[2]⋆ M. López-Caniego,[3,4] L. Toffolatti,[5] J. L. Sanz,[3] P. Vielva[3] and D. Herranz[3]

[1]*SISSA–ISAS, via Beirut 4, I-34014 Trieste, Italy*
[2]*Departamento de Matemáticas, Universidad de Oviedo, Avda. Calvo Sotelo s/n, 33007 Oviedo, Spain*
[3]*Instituto de Física de Cantabria (CSIC-UC), Avda. los Castros s/n, 39005 Santander, Spain*
[4]*Departamento de Física Moderna, Universidad de Cantabria, Avda. los Castros, s/n, 39005 Santander, Spain*
[5]*Departamento de Física, Universidad de Oviedo, Avda. Calvo Sotelo s/n, 33007 Oviedo, Spain*

ABSTRACT

We propose a new detection technique in the plane based on an isotropic wavelet family. This family is naturally constructed as an extension of the Gaussian–Mexican hat wavelet pair and for that reason we call it the Mexican hat wavelet family (MHWF). We show the performance of these wavelets when dealing with the detection of extragalactic point sources in cosmic microwave background (CMB) maps: a very important issue within the most general problem of the component separation of the microwave sky. Specifically, flat two-dimensional simulations of the microwave sky comprising all astrophysical components plus instrumental noise have been analysed for the channels at 30, 44 and 70 GHz of the forthcoming ESA *Planck* mission Low Frequency Instrument (LFI). We adopt up-to-date cosmological evolution models of extragalactic sources able to fit well the new data on high-frequency radio surveys and we discuss our current results on point-source detection by comparing them with those obtained using the Mexican hat wavelet (MHW) technique, which has been already proven a suitable tool for detecting point sources. By assuming a 5 per cent reliability level, the first new members of the MHWF, at their 'optimal scale', provide three point-source catalogues on half of the sky (at Galactic latitude $|b| > 30°$) at 30, 44 and 70 GHz of 639, 387 and 340 extragalactic sources, respectively. The corresponding flux detection limits are 0.38, 0.45 and 0.47 Jy. By using the same simulated sky patches and at the same frequencies as before, the MHW at its optimal scale provides 543, 322 and 311 sources with flux detection limits of 0.44, 0.51 and 0.50 Jy, respectively (5 per cent reliability level). These results show a clear improvement when we use the new members of the MHWF and, in particular, the MHW2 with respect to the MHW.

Key words: techniques: image processing – cosmic microwave background.

1 INTRODUCTION

The component separation of the microwave sky is one of the relevant problems of cosmic microwave background (CMB) data analysis. Before extracting the very important information encoded in the CMB anisotropies (e.g. cosmological parameters, evolution scenario, probability distribution of the primordial perturbations), it is critical to separate the pure CMB signal from other *contaminant* emissions also present in the microwave sky. These contaminants are known as foregrounds. Foregrounds are usually divided in two categories: galactic emissions (dust, free–free and synchrotron) and compact sources (galaxy clusters and extragalactic sources). A de-

tailed description of the expected contamination level (both in terms of frequency and angular power spectrum) for each foreground is discussed in Tegmark et al. (2000). The emission due to extragalactic point sources [radio and infrared (IR) galaxies seen as point-like objects due to their very small projected angular size as compared with the typical experimental resolutions] has very specific characteristics. First, whereas galactic foregrounds are highly anisotropic (most of their emissions are concentrated inside the galactic plane), extragalactic point sources are isotropically distributed in the sky (Franceschini et al. 1989; González-Nuevo, Toffolatti & Argüeso 2005) and display an angular size determined by the full width half maximum (FWHM) of the observational beam.

Secondly, whereas the energy spectrum of the galaxy clusters emission at CMB frequencies is very well known and it is the same

⋆E-mail: gnuevo@sissa.it (JG-N); argueso@uniovi.es (FA)

for all the clusters, the energy spectrum of each point source is given by the intrinsic characteristics of the physical processes that occur inside each galaxy and can be quite different from source to source.

Thirdly, whereas there are very good templates for the Galactic components,[1] not only about their spatial distribution, but also about their frequency dependence, our knowledge of the extragalactic point-source emission at microwave frequencies comes mostly from models based on observations at lower and higher frequencies (Guiderdoni et al. 1998; Toffolatti et al. 1998; Dole, Lagache & Puget 2003; Granato et al. 2004). This makes the detection of as many extragalactic sources as possible in CMB anisotropy maps a very important task by itself and not only in terms of *map cleaning*.[2]

Albeit very useful for studying the brightest sources in the CMB sky, the very shallow survey (208 objects at fluxes $S \geqslant 1$ Jy) provided by the NASA *WMAP* satellite (Bennett et al. 2003a) does not allow a detailed analysis of the statistical properties of the observed source populations. The situation shall be partially clarified in the near future, thanks to the ground-based very large sky surveys (e.g. Australia Telescope Compact Array, Ryle Telescope) that have been already planned and partially completed (Waldram et al. 2003; Ricci et al. 2004) at $\nu \leqslant 30$ GHz. On the other hand, there is no planned large area survey at frequencies $\geqslant 30$ GHz, due to the limits of ground-based techniques. However, the current lack of data should be overcome thanks to the all-sky surveys at nine frequencies (from 30 to 860 GHz) that should be completed by the ESA *Planck* satellite (Mandolesi et al. 1998; Puget et al. 1998) during the year 2008. *Planck* surveys, intended to pick up from several hundreds to thousands of extragalactic sources (De Zotti et al. 2004), shall be unique in this new observational window: they will span a larger frequency interval and shall be also much more sensitive than the *WMAP* ones. Moreover, the complementary samples of point sources provided by the ESA *Herschel* satellite, which will be launched jointly with *Planck* for observing the sky at higher (mid- and far-IR) frequencies, should help in clarifying the nature of source populations observed by *Planck* High Frequency Instrument (HFI) and of high-redshift sources, in particular.

For all the above reasons and for the fact that, at mm/submm frequencies, the emission of extragalactic sources is at a minimum (De Zotti et al. 1999; making more difficult their identification and separation from the other astrophysical components), of great interest is the study and development of new techniques for the detection of extragalactic point sources, as well as the improvement of existing ones by reaching fainter fluxes.

In particular, wavelet techniques have shown a very good performance to solve this problem. Wavelets have been applied to many different fields in physics during the last decade, e.g. geophysics, fluids and astrophysics/cosmology.

A relevant approach was also introduced by Marr & Hildreth (1980) considering the continuous wavelet transform. In the latter case, there is a redundance of wavelet coefficients, but analysis of signals and images can also be performed. The basic idea, when we apply wavelets in R^N, is the decomposition of a function $f(\boldsymbol{x})$ on a basis that incorporates the local and scaling behaviour of the

function. Therefore, given the domain of definition, the continuous transform involves translations and dilations

$$w(\boldsymbol{b}, R) = \int \mathrm{d}\boldsymbol{x}\, f(\boldsymbol{x})\Psi(\boldsymbol{x}; \boldsymbol{b}, R), \tag{1}$$

with

$$\Psi(\boldsymbol{x}; \boldsymbol{b}, R) \equiv \frac{1}{R^N} \psi\left(\frac{|\boldsymbol{x} - \boldsymbol{b}|}{R}\right), \tag{2}$$

where ψ and w are the mother wavelet and wavelet coefficient, respectively, and R is the scale (we assume an isotropic wavelet; see, for example, Sanz et al. 1999).

A particular and relevant case is the Mexican hat wavelet (MHW) defined on R^2:

$$\psi(x) \propto (2 - x^2)\mathrm{e}^{-x^2/2}, \quad x \equiv |\boldsymbol{x}|. \tag{3}$$

This wavelet and its extension to the sphere have been extensively used in the literature to detect structure on a 2D image: e.g. in astrophysics, for detecting point sources in CMB maps (Cayón et al. 2000; Vielva et al. 2001, 2003) and galaxy clusters in X-ray images (Damiani et al. 1997), by using the signal amplification when going from real to wavelet space.

The MHW is a very useful and powerful tool for point-source detection for the following reasons.

(i) It has an analytical form that is very convenient when making calculations and that allows us to implement fast algorithms.

(ii) It is well suited for the detection of Gaussian structures because it is obtained by applying the Laplacian operator to the Gaussian function.

(iii) It amplifies the point sources with respect to the noise. Moreover, by changing the scale of the Mexican hat it is possible to control the amplification until an optimum value is achieved.

(iv) In any case, to obtain the optimal amplification it is not necessary to assume anything about the noise. In Vielva et al. (2001), it was shown that the optimal scale can be easily obtained by means of a simple procedure for any given image. Therefore, the MHW wavelet is a very robust tool.

We want to further develop the idea behind the Mexican hat by exploring a generalization of this wavelet that keeps these good properties while improving the detection. In this paper, we introduce a natural generalization of the Gaussian–MHW pair on R^2 that satisfies the properties mentioned above. This generalization will allow us to improve the number of point-source detections in CMB maps, controlling the fraction of false detections (reliability). In Section 2, we develop our technique and give some properties of the Mexican hat wavelet family (MHWF). In Section 3, we study first the case of a point source embedded in white noise. Subsequently, we apply the method to the problem of point-source detection in CMB maps, considering in particular the Low Frequency Instrument (LFI) of the *Planck* mission. Realistic numerical simulations and a comparison with standard (wavelet space) techniques are performed. Finally, the main conclusions are drawn in Section 4.

2 THE MEXICAN HAT WAVELET FAMILY

The MHW on the plane is obtained by applying the Laplacian operator to the 2D Gaussian. If we apply the Laplacian to the MHW we obtain a new wavelet and if we iterate the process we get a whole family of wavelets: we call these wavelets the MHWF. We choose the normalization so that the sum of the Fourier transforms

---

[1] See, for example, the recently released *Planck* 'Galactic Reference Sky Model' prepared by the *Planck* Working Group 2, *Component Separation*, and available on the web page http://www.planck.fr/heading79.html.

[2] Obviously, all-sky samples made up of thousands of sources, hopefully available in the near future with *Planck*, will be unique in providing knowledge on the emission and cosmological evolution properties of the different underlying source populations, in this almost unexplored frequency domain (De Zotti et al. 2006).
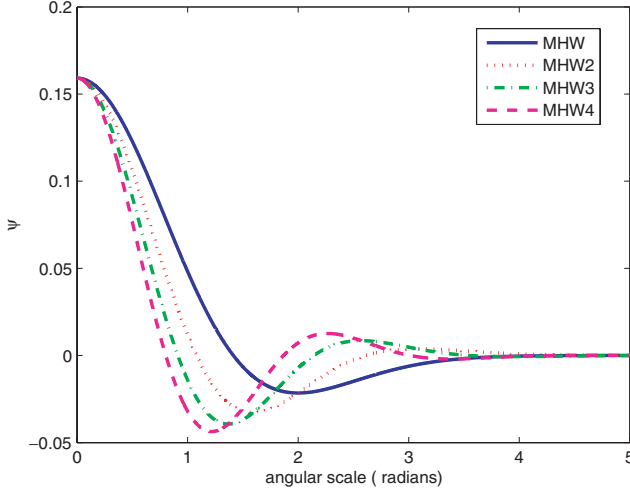
Figure 1. Radial profile of the Mexican hat wavelet (solid line), MHW2 (dotted line), MHW3 (dash-dotted line), MHW4 (dashed line).

of all these wavelets and of the Gaussian filter is one. Therefore, any member of the family can be written in Fourier space as

$$\hat{\psi}_n(k) = \frac{k^{2n}e^{-k^2/2}}{2^n n!}. \tag{4}$$

The new wavelet expression in real space is

$$\psi_n(x) = \frac{(-1)^n}{2^n n!} \Delta^n \varphi(x), \tag{5}$$

where φ is the 2D Gaussian $\varphi(x) = \frac{e^{-x^2/2}}{2\pi}$ and we apply the Laplacian operator n times. Note that $\psi_1(x)$ is the standard MHW.

The first four members of the MHWF are shown in real space in Fig. 1. Because the MHW has proven very useful for dealing with point-source detection, we will explore the performance of the MHWF in this practical application.

Let us consider a field $f(\boldsymbol{x})$ on the plane R^2, where $\boldsymbol{x}$ is an arbitrary point. One can define the wavelet coefficient at scale R at the point $\boldsymbol{b}$ in the form given by equations (1) and (2) with $N = 2$.

The Fourier transform of $\psi_n(x)$ is

$$\hat{\psi}_n(k) = \int_0^\infty dx\, x J_0(kx) \psi_n(x), \tag{6}$$

where $\boldsymbol{k}$ is the wave number, $k \equiv |\boldsymbol{k}|$ and J_0 is the Bessel function of the first kind.

The wavelet coefficients $w_n(\boldsymbol{b}, R)$ for each member of the MHWF can be obtained in the following form:

$$w_n(\boldsymbol{b}, R) = \int d\boldsymbol{k} e^{-i\boldsymbol{k}\cdot\boldsymbol{b}} f(\boldsymbol{k})\hat{\psi}_n(kR). \tag{7}$$

This expression can be rewritten (we assume the appropriate differential and boundary conditions for the field f) as

$$w_n(\boldsymbol{b}, R) = \int d\boldsymbol{x}\, [\Delta^n f(\boldsymbol{x})]\varphi\left(\frac{|\boldsymbol{x} - \boldsymbol{b}|}{R}\right). \tag{8}$$

Hence, the wavelet coefficient at point $\boldsymbol{b}$ can be interpreted as the filtering by a Gaussian window of the invariant $(2n)^{\text{th}}$ differences of the field f. We are then decomposing the field (image) with this wavelet family and analysing it at different resolution levels.

3 SOURCE DETECTION WITH THE MHWF

The MHW was applied with great success to the problem of detecting extragalactic sources in flat CMB maps (Cayón et al. 2000;

Vielva et al. 2001). The method was extended to the sphere (Vielva et al. 2003) and applied successfully to detailed simulations of maps at the *Planck* frequencies and with the characteristics of the *Planck* experiment. In all these cases, the MHW and its extension to the sphere were used as a filter at different scales, enhancing the signal-to-noise ratio for the sources and allowing us a very efficient detection and a good determination of the source flux. In the following, we will test the MHWF, as previously defined, for source detection.

3.1 Source detection in white noise maps

A basic point when we use a filter for source detection is how the signal-to-noise ratio of the sources in the filtered map is increased with respect to that of the original map: this effect is called amplification. In our first example, we consider a point source with a Gaussian profile embedded in white noise (i.e. a homogeneous and isotropic random field with a constant power spectrum). We consider a flat pixelized image consisting of a filtered source plus white noise added at any pixel and then we calculate the amplification produced by the MHWF in this particular case. Let us first calculate analytically (see equation 7) the wavelet coefficients obtained by filtering with any member of the MHWF a source of temperature $T(x) = T_0 e^{-x^2/2\gamma^2}$, where the source of temperature T_0 has been previously convolved with a Gaussian beam of dispersion γ. We obtain the following coefficients at $\boldsymbol{b} = 0$ (the point of maximum temperature of the source):

$$w_n = \frac{T_0 \beta^{2n}}{(1 + \beta^2)^{n+1}}, \tag{9}$$

where $\beta = \frac{R}{\gamma}$ and R is the wavelet scale. Now we will calculate the rms deviation σ_{w_n} of the background (white noise) filtered with a wavelet of scale R as a function of the rms deviation σ of the background:

$$\sigma_{w_n} = \frac{\sigma l_p \sqrt{(2n)!}}{R\pi 2^n n!}, \tag{10}$$

where l_p is the pixel size. The amplification λ_n is defined as

$$\lambda_n = \frac{w_n/\sigma_{w_n}}{T_0/\sigma}. \tag{11}$$

Then, the amplification for the white noise case can be written as

$$\lambda_n = \frac{\beta^{2n+1}\gamma\pi 2^n n!}{(1 + \beta^2)^{n+1}l_p\sqrt{(2n)!}}. \tag{12}$$

We can obtain the scale of maximal amplification for each wavelet, deriving with respect to β and equating to zero. We obtain $\beta_{\max} = \sqrt{2n + 1}$, so that the optimal scale depends on n and is $R_{\max} = \sqrt{2n + 1}\gamma$. The maximum amplification only depends on n and can be written as

$$\lambda_{\max} = \frac{(2n + 1)^{(n+\frac{1}{2})}n!\,\pi\gamma}{2(n + 1)^{n+1}\sqrt{(2n)!}\,l_p}. \tag{13}$$

If we calculate $\lambda_{\max}$ according to this formula, we obtain a maximum value for $n = 0$, a Gaussian filter with $R = \gamma$. So, the optimal amplification is reached when we filter again with a Gaussian beam of the same dispersion as the original one. The maximum amplification for other members of the MHWF decreases slowly as the index n increases.

3.2 Source detection in CMB maps

We have carried out a simple calculation for the case of a point source embedded in a white noise background. However, we are more interested in the realistic conditions of a CMB experiment in which the source is embedded in the CMB, the Galactic foregrounds and the detector Gaussian noise. A way to analyse the amplification given by equation (11) is to carry out simulations of the CMB maps with all the components and to measure the rms deviations σ_{w_n} and σ. The expression for w_n is the one given by equation (9).

For detecting point sources and for calculating the amplification factor of a source embedded in a realistic CMB map, we have carried out simulations of CMB 2D maps of 12.8×12.8 deg^2, generated with the cosmological parameters of the standard model (Spergel et al. 2003). We have then added the relevant Galactic foregrounds (free–free, synchrotron and dust emission) by using the *Planck* Galactic Reference Sky Model, provided by the members of the *Planck* Working Group 2.

In order to give the (hopefully) most realistic numbers of detected extragalactic point sources, we have adopted the cosmological evolution model for sources recently presented by De Zotti et al. (2005) for predicting the numbers of galaxies in our simulations. This new model, which takes into account the new data coming from high-frequency ($\sim$20–30 GHz) radio surveys of extragalactic sources and that discusses all source populations that can contribute to number counts at LFI frequencies, has proven capable of giving a better fit than before to all the currently published source number counts and related statistics at $\nu \leqslant 30$ GHz coming from different surveys (Bennett et al. 2003b; Mason et al. 2003; Waldram et al. 2003; Ricci et al. 2004; Cleary et al. 2005).

Because we are especially interested in applying our new method to the maps that will be provided by the *Planck* mission in the near future and given that we can be very confident in the input source model counts, we have considered the specific conditions of the LFI *Planck* channels, which operate at 30, 44 and 70 GHz.[3]

According to formula (9), we can calculate the temperature of the point source at its central pixel in the filtered maps for each wavelet and at any scale, given the original temperature. We find complete agreement between the values obtained from the formulae and the results coming from our simulations for all the wavelets and scales involved. Our next step is to calculate the amplification for different members of the MHWF and for different values of the wavelet scale, R; our goal is to obtain the *optimal scales* for the different wavelets used and to compare them for source detection. At 30 GHz, the maximum amplification for the MHW is 2.21. This amplification is reached at the optimal scale $R = 9.1$ arcmin. For the other members of the family, MHW2, MHW3 and MHW4, the amplifications are: 2.68, 2.87, 2.94 and are obtained at the optimal scales $R = 13.5$, 17.4 and 20.5 arcmin, respectively.

At 44 GHz, the maximum amplification for the MHW is 2.3 and it is obtained at the scale $R = 7.3$ arcmin. For the members MHW2, MHW3 and MHW4, the amplifications are 2.74, 2.83, 2.80 and correspond to the scales $R = 11.2$, 14.1 and 16.5 arcmin, respectively. In Fig. 2 we show, as an example, the amplification, λ, obtained at different scales with the first four members of the MHWF at
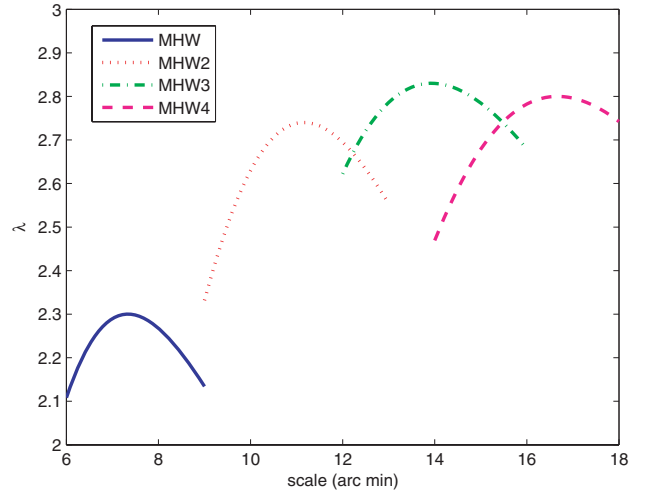
Figure 2. Amplification λ of a point source in 44 GHz CMB maps for the MHW (solid line), MHW2 (dotted line), MHW3 (dash-dotted line) and MHW4 (dashed line) as a function of the scale in arcmin.

44 GHz. At 70 GHz and for the MHW, MHW2, MHW3 and MHW4 we find $\lambda = 2.59$, 2.79, 2.76, 2.69, and these amplifications are obtained at the scales $R = 5.3$, 7.6, 9.4 and 10.9 arcmin, respectively. All the tests done with members of the MHWF defined by higher n (see equation 5) show a lesser amplification at each of the three frequencies and this also happens when a Gaussian filter is used. For this reason, we limited our study of the capability of source detection of the MHWF to the first four members of the family.

We have then used the MHW2, MHW3 and MHW4 at the optimal scales to detect point sources in the maps at 30, 44 and 70 GHz, comparing the results with those obtained with the MHW. Our detection method is quite simple, we carry out enough simulations (10×126) of 2D sky patches to cover 10 times half the sky at $|b| > 30°$. As previously stated, the simulations include point sources, Galactic foregrounds, CMB and the detector noise.

In Fig. 3 (top-left panel) we show one of the simulated CMB maps we analysed at 44 GHz and the corresponding map of extragalactic point sources only (top right). The same map, filtered with the MHW and with the MHW2 at their optimal scales, is shown in the central-left and central-right panels, respectively. In the bottom-left and bottom-right panels, we show the same original simulated map filtered with the MHW3 and the MHW4, respectively. In all the panels, the brightest (detected) sources are shown as red spots in the filtered maps (given the adopted colour scale of the maps; see caption); because we have simulated sky patches of 12.8×12.8 deg^2, only a few (very bright) sources are detected in each sky patch. Thus, from only one map, it is not possible to tell visually apart the differences in the number of detections after filtering with one specific member of the family or with another one. However, the map filtered with the MHW (central-left panel) is clearly noisier than the other maps filtered with other members of the family. This is due to the fact that the variance of this map is $\simeq$10 per cent higher than in the other cases.

After filtering each simulation with the corresponding wavelet at the optimal scale, we use equation (9) to calculate the flux at any pixel. First, we select those pixels corresponding to maxima above 300 mJy (because for lower flux detection limits the fraction of spurious sources, as defined below, is very high). Then we compare these maxima with the fluxes of the sources in the simulations (beam filtered). We consider a detection as real when the following
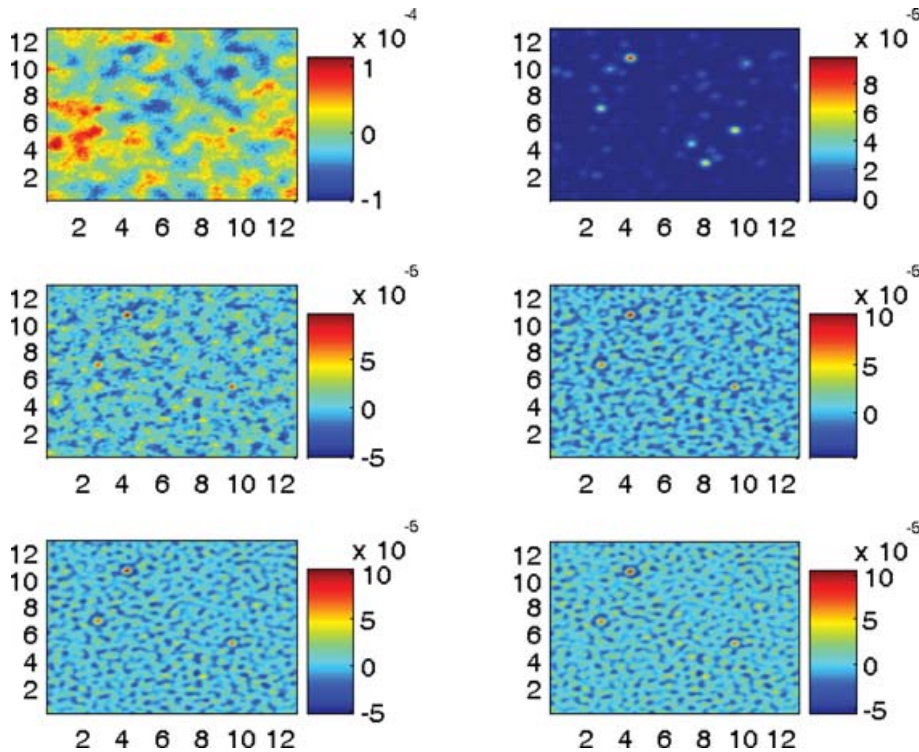
Figure 3. 44-GHz maps. Top-left panel: CMB+ sources+ noise+ foregrounds map (total map). Top-right: the corresponding map of simulated extragalactic point sources only. From central-left to bottom-right, the panels show the total map filtered with the MHW, MHW2, MHW3, MHW4 at the corresponding optimal scale, respectively. The colour scale is in $\delta T/T$ units. The angular scale is in degrees.

criteria are satisfied: (i) the distance between each maximum and the corresponding simulated source is FWHM/2; and (ii) the relative difference between the estimated and the real flux is less than 100 per cent. The maxima (above 300 mJy) that do not fulfil these criteria are considered as spurious sources.

The average number of sources correctly detected in half of the sky (see Table 1) with the MHW, MHW2, MHW3 and MHW4, respectively, are: 873, 850, 846 and 845 at 30 GHz; 695, 673, 671 and 674 at 44 GHz; and 634, 622, 623 and 627 at 70 GHz. The average number of spurious sources with the MHW, MHW2, MHW3 and MHW4, respectively, are: 1230, 431, 409 and 526 at 30 GHz; 4538, 2008, 1988 and 2366 at 44 GHz; and 8082, 4980, 5236 and 6254 at 70 GHz. Because the number of spurious sources for the assumed flux limit (300 mJy) is very high, it seems more appropriate to impose a level of reliability (fraction of spurious sources), e.g. 5 per cent. With this reliability level, the number of real detections for the MHW, MHW2, MHW3 and MHW4 are: 543, 639, 583 and 418 at 30 GHz; 322, 387, 366 and 275 at 44 GHz; and 311, 340, 331 and 288 at 70 GHz.

In Table 1, these results at 30, 44 and 70 GHz are shown together with other relevant information about the detection process: the flux limit for which the reliability is 5 per cent, the flux over which the source catalogue is 95 per cent complete, the number of sources detected in the 95 per cent completeness catalogue and the average of the absolute value of the flux determination relative error. In the table, we write the average results and the rms deviations (from 10 half skies).

We want to remark on the following results.

(i) The average number of detections above 300 mJy is a little higher for the MHW than for the other members of the MHWF, but the number of spurious sources is much higher.

(ii) The number of detected sources with a 5 per cent reliability is higher for the MHW2 than for the other members. When we compare with the MHW, we see a clear increase in the real detections: this increase is $\simeq$18 per cent (30 GHz), $\simeq$20 per cent (44 GHz), $\simeq$9 per cent (70 GHz). The perfomance of the MHW4 is the worst in this respect.

(iii) We also note that the average error in the flux determination is always below $\simeq$25 per cent, being lower for the new wavelets than for the MHW.

According to these results, the most efficient strategy is to study all these wavelets, MHWn with $n \leqslant 4$, and choose the one that better fulfils the detection criterion. Of course, this conclusion can be applied only to the kind of maps used here; in other *Planck* channels, for example, the best results may be obtained with other MHWn. In general, the use of the MHWF allows us to determine and (then) apply the most efficient wavelet filter, of the same family, for detecting point sources embedded in realistic CMB maps. We want to point out that the proposed method could be applied to the real maps provided by the *Planck* satellite, because it is easy to calculate, in each particular case, the amplification and the optimal scales for source detection.

In Fig. 4 (top-left panel), we plot the percentage of spurious sources against the flux detection limit for the different wavelets at 30 GHz. In the middle-left panel we show the same results at 44 GHz and in the bottom-left panel at 70 GHz. As it can be seen, this percentage is higher for the MHW and the MHW4 than for the other wavelets. In the same figure, we plot the absolute error in the flux determination against the flux detection limit at 30 GHz (top-central panel), 44 GHz (middle-central panel) and 70 GHz (bottom-central panel). As it is clear from the figure, this error is lower for

Table 1. Point-source detections at 30, 44 and 70 GHz in half of the sky, 2π sr, above 300 mJy, for several members of the MHWF. In each column, we indicate the average and the rms deviation (in curly brackets) of some relevant quantities calculated by the simulations on sky patches corresponding to 10 half skies. In the first column, we show the number of detections, $N_{\rm d}$, in the second one the number of spurious sources, $N_{\rm sp}$, and in the third one we list the fluxes at which the recovered source catalogues are complete at the 95 per cent level. The number of detected sources brighter than these fluxes are shown in the fourth column. In the fifth and sixth columns, the fluxes above which the catalogues have a 5 per cent reliability and the corresponding numbers of detected sources are shown, respectively. Finally, we show in the last column the average of the absolute value of the relative error (in per cent) in the flux determination.

	$N_{\rm d}$	$N_{\rm sp}$	S_{95} (Jy)	N_{95}	S_5 (Jy)	N_5	$\lvert\Delta S\rvert/S$ (per cent)
30 GHz							
MHW	873(30)	1230(39)	0.33(0.01)	637(26)	0.44(0.01)	543(26)	21.9(0.9)
MHW2	850(27)	431(32)	0.34(0.02)	632(27)	0.38(0.01)	639(31)	18.6(0.5)
MHW3	846(34)	409(36)	0.34(0.01)	628(24)	0.41(0.02)	583(42)	18.1(0.4)
MHW4	845(35)	526(39)	0.34(0.01)	626(28)	0.51(0.04)	418(63)	18.4(0.5)
44 GHz							
MHW	695(28)	4538(66)	0.35(0.01)	459(32)	0.51(0.01)	322(22)	25.5(0.6)
MHW2	673(26)	2008(43)	0.35(0.01)	462(24)	0.45(0.01)	387(21)	21.7(0.6)
MHW3	671(26)	1988(39)	0.34(0.01)	467(31)	0.46(0.02)	366(37)	21.6(0.7)
MHW4	674(28)	2366(43)	0.35(0.01)	466(33)	0.56(0.06)	275(54)	22.1(0.7)
70 GHz							
MHW	634(24)	8082(72)	0.33(0.01)	452(23)	0.50(0.01)	311(24)	23.5(0.9)
MHW2	622(30)	4980(81)	0.34(0.01)	447(31)	0.47(0.01)	340(31)	21.4(0.8)
MHW3	623(27)	5236(108)	0.34(0.01)	443(34)	0.47(0.01)	331(30)	21.7(0.9)
MHW4	627(26)	6254(105)	0.34(0.01)	444(36)	0.53(0.03)	288(38)	22.3(0.9)
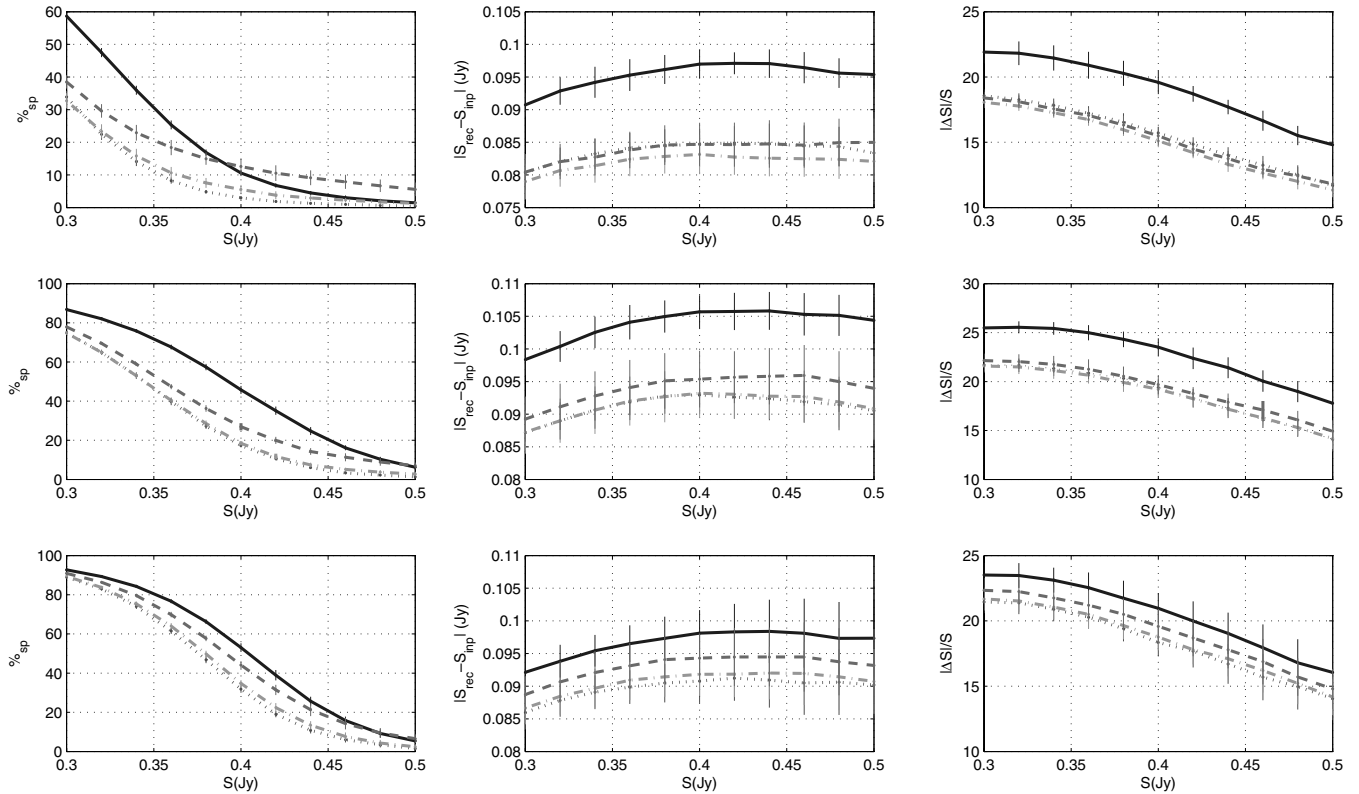
Figure 4. Top-left panel: the percentage of spurious sources at 30 GHz is plotted against the flux detection limit. Top-central panel: the average of the absolute value of the error in the flux determination at 30 GHz is plotted against the flux limit. Top-right panel: the average of the absolute value of the relative error (percentage) in the flux determination at 30 GHz is plotted against the flux limit. In each panel, the average of 10 half skies together with the rms error bars are shown for the MHW (solid line), MHW2 (dotted line), MHW3 (dash-dotted line) and MHW4 (dashed line). Middle-/bottom-left panel: the same plot as in the top-left panel at (44/70) GHz. Middle-/bottom-central panel: the same plot as in the top-central panel at (44/70) GHz. Middle-/bottom-right panel: the same plot as in the top-right panel at (44/70) GHz.

the new members than for the standard MHW. Finally, in the right panels, we plot the relative error in the flux determination for the three frequencies; the error percentage is also lower for the MHW2 and MHW3 than for the other wavelets.

We have analysed (realistic) simulated CMB maps at three frequencies, corresponding to the LFI channels of the *Planck* mission, but the present results encourage us to test the proposed method at other CMB frequencies, in forthcoming papers. Moreover, the method could be extended to the sphere, just by applying the stereographic projection (Cayón et al. 2001; Martínez-González et al. 2002) to the MHWF and then by using it to analyse spherical CMB maps (Vielva et al. 2003).

4 CONCLUSIONS

We have considered a natural generalization of the MHW on the plane, R^2, based on the iterative application of the Laplacian operator to the MHW. We have called this group of wavelets the MHWF.

The MHWF can therefore be applied to the analysis of flat two-dimensional images and, in particular, to current and forthcoming CMB maps provided by the plethora of the existing (and planned) experiments. Our main goal is to test this wavelet family in one typical application, point-source detection in CMB anisotropy maps, and to compare our results with those obtained by the use of the MHW. The detection of as many extragalactic sources as possible in CMB maps is an important issue per se, and not only for the purpose of map cleaning, for it allows the construction of catalogues of point-source populations at frequencies where there are only few and sparse data available at the present time.

The main reason why wavelets perform well when detecting point sources is that they amplify the ratio between the point-source flux density and the dispersion of the background. For a simple background, such as white noise, this amplification can be calculated easily, see equations (12) and (13). In this very simple case, the maximum amplification is obtained with the Gaussian filter.

However, because we want to propose a detection method that could be applied to real CMB anisotropy maps, we have carried out realistic simulations of the CMB sky including primordial CMB anisotropies, point sources, instrumental (thermal Gaussian) noise and all the relevant foregrounds. To test the method, we have chosen the three channels of the *Planck* LFI, 30, 44 and 70 GHz (using the characteristics currently established for them). This choice is also due to the fact that, in this frequency interval, it is currently possible to simulate a very realistic number of bright extragalactic point sources in the sky, by exploiting the cosmological evolution model of De Zotti et al. (2005). In all the cases, we have considered 10 × 126 maps of 12.8×12.8 deg^2 for covering 10 times half the sphere at high Galactic latitude. After filtering with the MHWF, we select the maxima in such maps as possible candidates and compare them with the maxima in the beam filtered source maps.

We consider a detection as real if the following two criteria are satisfied: (i) the distance between the maxima and the corresponding sources is FWHM/2; and (ii) the relative difference between the estimated and the real flux is less than 100 per cent. In this way, we construct a source catalogue above 300 mJy of real detections. The other maxima are considered as spurious sources. From this catalogue, we can draw the following main conclusions.

(i) We have compared the performance of the new members of the MHWF for point-source detection with that of the MHW alone, at their optimal scale (Cayón et al. 2000; Vielva et al. 2001). Our results clearly show that, although the number of detections is sim-ilar, the *number of spurious sources is much lower* ($\leqslant 50$ per cent) for the new wavelets than for the MHW.

(ii) By assuming a 5 per cent reliability, the *number of detected sources* obtained by filtering with the new wavelets and, in particular, with the MHW2 is *higher* than the number obtained with the original MHW (see Section 3.2). We detect (639/543) sources (MHW2/MHW) at 30 GHz, (387/322) sources (MHW2/MHW) at 44 GHz and (340/311) sources (MHW2/MHW) at 70 GHz. The 5 per cent reliability flux limit is (380/440) mJy at 30 GHz, (450/510) mJy at 44 GHz and (470/500) mJy at 70 GHz.

(iii) The average of the absolute value of the relative error ($|\Delta S|/S$) is *lower* for the new members of the MHWF than for the MHW. This average value is (18.1/21.9) per cent at 30 GHz, (21.6/25.5) per cent at 44 GHz and (21.4/23.5) per cent at 70 GHz.

In general, we can see a clear improvement in the number of detections and in the flux estimation when we apply the new wavelets. Further information can be seen in Table 1. In Fig. 4, we can also see the percentage of spurious sources and the average absolute and relative errors in the flux determination plotted against the flux limit for the different wavelets and frequencies.

The MHWF could be extended to the sphere in a straightforward way, by using a stereographic projection, allowing us to analyse all-sky CMB maps. CMB experiments other than *Planck* could also benefit from the source amplification performed by the MHWF.

REFERENCES

Bennett C. L. et al., 2003a, ApJ, 583, 1
Bennett C. L. et al., 2003b, ApJS, 148, 97
Cayón L., Silk J., 2001, MNRAS, 325, 1533
Cayón L. et al., 2000, MNRAS, 313, 757
Cayón L., Sanz J. L., Martínez-González E., Banday A. J., Argüeso F., Gallegos J. E., Górski K. M., Hinshaw G., 2001, MNRAS, 326, 1243
Cleary et al., 2005, MNRAS, 360, 340
Damiani F., Maggio A., Micela G., Sciortino S., 1997, ApJ, 483, 370
De Zotti G., Toffolatti L., Argüeso F., Davies R. D., Mazzotta P., Partridge R. B., Smoot G. F., Vittorio N., 1999, in Maiani L., Melchiorri F., Vittorio N., eds, AIP Conf. Proc. 476, EC-TMR Conf., 3K Cosmology. American Institute of Physics, Melville, p. 204
De Zotti G., Burigana C., Negrello M., Tinti S., Ricci R., Silva L., González-Nuevo J., Toffolatti L., 2006, in Del Toro Iniesta J. C., ed., Proc. Jenam 2004, The many scales in the Universe. Kluwer (Springer), Dordrecht, p. 45
De Zotti G., Ricci R., Mesa D., Silva L., Mazzotta P., Toffolatti L., González-Nuevo J., 2005, A&A, 431, 893
Dole H., Lagache G., Puget J.-L., 2003, ApJ, 583, 617
Franceschini A., Toffolatti L., Danese L., De Zotti G., 1989, ApJ, 344, 35

González-Nuevo J., Toffolatti L., Argüeso F., 2005, ApJ, 621, 1

Granato G. L., De Zotti G., Silva L., Bressan A., Danese L., 2004, ApJ, 600, 580

Guiderdoni B., Hivon E., Bouchet F. R., Maffei B., 1998, MNRAS, 295, 877

Mandolesi N. et al., 1998, Proposal for the Planck Low Frequency Instrument (LFI), ESA Science Report D(SCI)-98(03). ESA, Paris

Marr D., Hildreth E. C., 1980, Theory of Edge Detection, Proc. R. Soc. Lond., B, 207, 187–217

Martínez-González E., Gallegos J. E., Argüeso F., Cayón L., Sanz J. L., 2002, MNRAS, 336, 22

Mason B. S. et al., 2003, ApJ, 591, 540

Puget J. L. et al., 1998, Proposal for the 'Planck' High Frequency Instrument (HFI), ESA Science Report D(SCI). ESA, Paris

Ricci R. et al., 2004, MNRAS, 354, 305

Sanz J. L., Argüeso F., Cayón L., Martínez-González E., Barreiro R. B., Toffolatti L., 1999, MNRAS, 309, 672

Spergel D. N. et al., 2003, ApJS, 148, 175

Tegmark M., Efstathiou G., 1996, MNRAS, 281, 1297

Tegmark M., Eisenstein D. J., Hu W., de Oliveira-Costa A., 2000, ApJ, 530, 133

Toffolatti L., Argüeso Gómez F., de Zotti G., Mazzei P., Franceschini A., Danese L., Burigana C., 1998, MNRAS, 297, 117

Vielva P., Martínez-González E., Cayón L., Diego J. M., Sanz J. L., Toffolatti L., 2001, MNRAS, 326, 181

Vielva P., Martínez-González E., Gallegos J. E., Toffolatti L., Sanz J. L., 2003, MNRAS, 344, 89

Waldram E. M., Pooley G. G., Grainge K. J. B., Jones M. E., Saunders R. D. E., Scott P. F., Taylor A. C., 2003, MNRAS, 342, 915

This paper has been typeset from a TEX/LATEX file prepared by the author.